The Mechanism of NEDD8 Activation of CUL5 Ubiquitin E3 Ligases

Ryan J. Lumpkin, Alla S. Ahmad, Rachel Blake, Christopher J. Condon and Elizabeth A. Komives*

Department of Chemistry and Biochemistry, University of California, San Diego, 9500 Gilman Drive, La Jolla, CA 92092-0378.

*Corresponding author: Elizabeth A. Komives

Department of Chemistry and Biochemistry, University of California, San Diego, 9500 Gilman Drive, La Jolla, CA 92092-0378

Ph: (858) 534-3058

Email: ekomives@ucsd.edu

ORCID ID: 0000-0001-5264-3866

Running Title: How Nedd8 Activates E3 ligases

Abbreviations: Cullin RING E3 Ligases, CRLs; RING between RING E3 ligases, RBRLs; Ankyrin repeat and SOCS Box protein 9, ASB9; Hydrogen-Deuterium Exchange Mass Spectrometry, HDX-MS; Ubiquitin, Ub; Suppressor of Cytokine Signaling, SOCS; creatine kinase brain-type, CKB; Elongin B/Elongin C, ELOB/C; LC MS/MS, nanospray liquid chromatography coupled to tandem mass spectrometry.

Abstract

Cullin RING E3 Ligases (CRLs) ubiquitylate hundreds of important cellular substrates. Here we have assembled and purified the Ankyrin repeat and SOCS Box protein 9 CUL5 RBX2 Ligase (ASB9-CRL) *in vitro* and show how it ubiquitylates one of its substrates, CKB. CRLs occasionally collaborate with RING between RING E3 ligases (RBRLs) and indeed, mass spectrometry analysis showed that CKB is specifically ubiquitylated by the ASB9-CRL-ARIH2-UBE2L3 complex. Addition of other E2s such as UBE2R1 or UBE2D2 contribute to polyubiquitylation but do not alter the sites of CKB ubiquitylation. Hydrogen-deuterium exchange mass spectrometry (HDX-MS) analysis revealed that CUL5 neddylation allosterically exposes its ARIH2 binding site, promoting high affinity binding, and it also sequesters the NEDD8 E2 (UBE2F) binding site on RBX2. Once bound, ARIH2 helices near the Ariadne domain active site are exposed, presumably relieving its autoinhibition. These results allow us to propose a model of how neddylation activates ASB-CRLs to ubiquitylate their substrates.

Ubiquitin (Ub) is a post-translational modification that is installed by an Activating Enzyme (E1), which transfers the Ub to a Conjugating Enzyme (E2), and a Ligase (E3), which brings the target substrate together with the E2 (Figure 1A). Association of substrates with E3s leads to the covalent attachment of Ub onto substrate lysines and poly-Ub chains. Formation of poly-Ub chains may involve more than one E2 enzyme (1). Both mono-Ub and the various poly-Ub chains lead to distinct signals. Ubiquitin monomers can be polymerized at any of seven lysine residues or the first methionine residue. The manner in which differential ubiquitin signaling is achieved by the differential interactions of distinct chain linkages with the proteasome, ubiquitin-binding proteins and deubiquitinases (DUBs) is referred to as the ubiquitin code (1, 2). The K48 and K63 linkages are most abundant, and these are found as pure chains, mixed chains, and branched chains mammalian cells (3).Typically, proteasome-targeting is thought to be the function of K48-linked chains, although others such as K11- or K29-linked chains as well as multiple short chains can also function as proteasomal signals (4, 5).

E3 Ligases fall into three major groups: Homologous to E6-AP carboxyl terminus (HECT), Really Interesting New Gene (RING), and Ring-Between-RING Ligases (RBRL). RING E3s account for approximately 90% of known Ub Ligases, and Cullin-RING Ligases (CRLs) are the most common RING E3s. CRLs are multi-subunit complexes consisting of a substrate receptor, adaptor proteins, a Cullin protein (CUL1-5, CUL7), and a RING protein (RBX1 or RBX2). The RING protein associates with Ub-bound E2 enzymes to facilitate the direct transfer of Ub from the E2 to bound substrate proteins. CUL5 interacts specifically with RBX2(6).

CUL2 and CUL5 have been shown to bind Elongin B and Elongin C (ELOB/C), through which CUL2 binds vHL-box substrate receptors and CUL5 binds Suppressor of Cytokine Signaling (SOCS)-box substrate receptors (7). Here we focus on the 18-member Ankyrin Repeat and SOCS-box (ASB) adapter family; a large class of E3 ligase substrate receptors (6). Each of the 18 ASB family members bind ~10 proteins (8), which are possible substrates for ubiquitylation, although that remains to be demonstrated. The ASB proteins contain an ankyrin repeat domain

(9, 10), presumably involved in substrate binding, and a SOCS-box domain, which contains the conserved BC-box and CUL5-box motifs for binding to ELOB/C. ASB9 was shown to bind creatine kinases (CKB) and to induce their ubiquitylation and degradation in a SOCS-box dependent manner (11, 12). ASB9 binds a dimer of CKB at the first ankyrin repeat (13). Structure determination of the ASB9-ELOB/C complex (14) and modeling of CKB, CUL5 and RBX1 led to models of the full ligase that depicted CKB bound to ASB9 approximately 70 Å away from the E2~Ub complex on RBX1(15). We recently reported on a part of the structure of this ligase (16). A structure has recently been solved for Neddylated CUL1-SKP1, β-TRCP and a substrate peptide showing by strategic cross-linking how the RBX1-bound ubiquitylated E2D reaches the substrate (17). This structure reveals one of the many possible functions of Neddylation wherein the NEDD8 forms an interaction with the E2D.

Some CRLs have been shown to have two modes of action, one in which the E2 attached to the RBX is responsible for Ub transfer and a second in which an RBRL, either ARIH1 or ARIH2, performs the Ub transfer. The ARIHs are RBRLs with characteristics of both HECT and RING ligases (18). These E3s contain two RING domains and an In-between-RING domain, but unlike RING ligases, the E3s associate with a cysteine-reactive E2 enzyme, UBE2L3, which transfers Ub to the catalytic cysteine on the RBRL (19). ARIH1 has been shown to interact with CUL1-4 and is important for Ub transfer to some CRL substrates (20). ARIH2 specifically interacts with a basic patch on CUL5 via an acidic N-terminus of ARIH2 (21) and has been shown to be essential for Ub transfer by a CUL5 ligase to the substrate APOBEC3G (22). Binding to CRLs is thought to relieve autoinhibition of the RBRLs (21) enabling the RBRL to ubiquitinate the substrate on the CRL (23). ARIH2 was shown to co-precipitate with ASB9 in pulldown proteomics studies (24), and recently was shown to help ubiquitinate CKB in the presence of the ASB9-CRL (22). Structures of ARIH2 bound to CUL5 are not yet available and the mechanism by which neddylation of CUL5 promotes binding of ARIH2 remains unknown.

Here, we present biochemical, structural, and biophysical data on the purified ASB9-CRL we have assembled *in vitro*. We show that the ASB9-CRL does not significantly ubiquitylate CKB in the absence of ARIH2-UBE2L3~Ub. The requirement of ARIH2 for efficient ubiquitylation of CKB distinguishes the mechanism of the CUL5-containing ASB9-CRL from the CUL1-containing ligase for which a structure was recently determined (17). Neddylation of CUL5 is required for high affinity binding of ARIH2, consistent with Hydrogen-deuterium exchange mass spectrometry (HDX-MS) experiments showing that neddylation allosterically exposes the ARIH2 binding site on CUL5. Neddylation also reduces solvent exposure of the NEDD8 E2, UBE2F binding site on RBX2, consistent with the need to exchange UBE2F with another E2 for ubiquitylation once neddylation is completed. When added to the CKB-bound ASB9-CRL, ARIH2-UBE2L3~Ub is sufficient to add multiple Ub moieties to four lysines on CKB, and addition of other E2s such as UBE2R1 or UBE2D2 modulate the polyubiquitin linkage activity of the ligase, but not the sites of ubiquitylation on CKB. HDX-MS experiments show that binding of ARIH2 to CUL5 allosterically triggers opening of its auto-inhibited Ariadne domain. These results provide a mechanism of how neddylation of the ASB9-CRL promotes ARIH2 binding and RBX2 E2 selectivity as well as how the ARIH2 is activated upon binding to CUL5.

Methods

Expression vectors. Human ASB9-1 in pNIC-CTHF was obtained from the Structural Genomics Consortium and subcloned into pHis8 (Kan^R) with an N-terminal 8xHis tag. Human CKB was subcloned into pET11a (Amp^R) as previously described (13). Human ELOB (full-length) and ELOC (17-112) were obtained in pACYC (Cam^R) (Structural Genomics Consortium). Human CUL5 and Mouse RBX2 were obtained in pRSFDuet (Kan^R) with an N-terminal His tag, TEV cleavage site, and GB1 tag on CUL5 (gift from Nevan Krogan). 6xHis-GB1-TEV-CUL5 was subcloned into pET28a (Kan^R) and RBX2 was subcloned into pET11a (Amp^R).

Human UBA1 in pET21b (Amp^R) with an N-terminal 6xHis tag was obtained from Addgene (Plasmid #34965). Human UBE2D2 in pET-SUMO (Amp^R) with an N-terminal 6xHis tag and SUMO solubility tag was obtained from Addgene (Plasmid #60443) and was subcloned into pET28a with an N-terminal 6xHis tag and TEV cleavage site. Human UBE2R1 in pDEST17 with an N-terminal 6xHis tag was obtained from Addgene (Plasmid #18674). Human Ub in pcDNA3 (Amp^R) with an N-terminal HA tag was obtained from Addgene (Plasmid #18712) and subcloned into pET28a (Kan^R) with an N-terminal 6xHis tag and TEV cleavage site. Human NAE1 and UBA3 were obtained in pGEX4T1 (Amp^R) with a GST tag (gift from Brenda Schulman). Human UBE2F in pDEST17 (Amp^R) with an N-terminal 6xHis tag was obtained from Addgene (Plasmid #15800) and was subcloned into pET28a (Kan^R) with an N-terminal 6xHis tag and TEV cleavage site. Human NEDD8 in pcDNA3 (Amp^R) with an N-terminal HA tag was obtained from Addgene (Plasmid #18711) and was subcloned into pET28a (Kan^R) with an N-terminal His tag. Codon-optimized human ARIH2 was synthesized with an N-terminal 6xHis tag, MBP solubility tag, and TEV cleavage site, and it was subcloned into pET11a (Amp^R) (GENEWIZ, Inc.). Codon-optimized human UBE2L3 was synthesized and subcloned into pET28a (Kan^R) with an N-terminal 6xHis tag and TEV cleavage site. TEV Protease was obtained in pRK793 (Amp^R) with an N-terminal MBP solubility tag, TEV cleavage site, and 6xHis tag (Gift from César Ramirez).

Protein Expression. ASB9 was co-expressed with ELOB/C and/or CKB using sequential transformation with appropriate vectors (above) into BL21 *E. coli* cells for ASB9-CKB, ASB9-ELOB/C, and ASB9-CKB-ELOB/C protein complexes. Vectors containing ELOB/C, CKB, or both were transformed into competent BL21 cells after which those cells were made competent again. ELOB/C in pACYC was selected for by Chloramphenicol (CAM) resistance, and CKB in pET11a was selected for by Ampicillin (AMP) resistance. The vector for expression of ASB9 was transformed into ELOB/C + CKB – containing BL21 cells and plated on a Kanamycin (KAN)-CAM-AMP LB agar plate. The pET28a vector for expression of CUL5 and the pET11a vector for expression of RBX2 were co-transformed into ELOB/C - containing BL21 cells and plated on a

KAN-CAM-AMP LB agar plate for co-expression of CUL5/RBX2/ELOB/C. Vectors for expression of UBE1 and Ub were co-transformed into BL21 cells and plated on a KAN-AMP LB agar plate for co-expression of UBE1/Ub. Vectors for expression of UBE2D2, UBE2L3, UBE2F, Ub and Nedd8 were transformed individually into BL21 cells and plated on KAN LB agar plates. Vectors for expression of NAE1/UBA3, UBE2R1, and ARIH2 were transformed individually into BL21 cells and plated on AMP LB agar plates.

All proteins were expressed as follows. A 5 mL M9-ZN (1.5 x M9 salts, NZ-Amine media, 0.8% Dextrose, 1 mM $MgSO_4$, 0.2 mM $CaCl_2$) overnight culture was inoculated with a single colony from the plate. A 20 mL M9-Zn starter culture was inoculated with 2 mL of the overnight culture and grown for 3 hours at 37 °C. The 1 L M9-ZN growth culture was inoculated with the entire 20 mL starter culture and grown until OD_{600} = 0.8. After placing the cultures on ice for 15 min, protein expression was induced by addition of IPTG to a final concentration of 0.5 mM, and the cultures were transferred to an 18 °C incubator for 16-18 hours. Because RBX2 and ARIH2 contain Zn binding domains, the cultures containing either of those proteins were brought to 200 μM Zn by addition of a 1 M solution of $ZnCl_2$ just prior to induction.

Protein Purification. Cells from 1 L of culture were pelleted by centrifugation at 5000 rpm for 10 minutes, then re-suspended in 40 mL Resuspension Buffer (50 mM Tris-HCL pH 8.0, 100 mM NaCl, 10 mM Imidazole pH 8.0, 2 mM β-mercaptoethanol, 5% Glycerol) with Protease Inhibitor Cocktail (Sigma P2714) and 5 mM PMSF. Cells were lysed on ice by sonication with ten 30 seconds pulses with 45 seconds cooldown between each pulse. The lysate was clarified by centrifugation at 13000 rpm for 45 minutes. The clarified lysate was incubated with 2 mL Ni-NTA (in Resuspension Buffer) for 2 hours at 4 °C with rocking. Ni-NTA beads were pelleted by centrifugation at 700 x g for 5 minutes. The supernatant was discarded, and the beads were washed with 10 mL Wash Buffer (50 mM Tris-HCL pH 8.0, 100 mM NaCl, 25 mM Imidazole pH 8.0, 2 mM β-mercaptoethanol, 5% Glycerol) for 30 minutes at 4°C. Ni-NTA beads were again pelleted by centrifugation at 700 x g for 5 minutes. The supernatant was discarded, and the beads

were washed with 10 mL Elution Buffer (50 mM Tris-HCL pH 8.0, 100 mM NaCl, 250 mM Imidazole pH 8.0, 2 mM β-mercaptoethanol, 5% Glycerol) for 30 minutes at 4 °C. Ni-NTA beads were again pelleted by centrifugation at 700 x g for 5 minutes. The supernatant was transferred to a 12-14 kDa Dialysis bag and dialyzed overnight in Dialysis Buffer (20 mM Tris-HCL pH 8.0, 100 mM NaCl, 5% Glycerol, 1 mM DTT). Samples were concentrated to 2 mL and purified using size-exclusion chromatography over a Superdex S200 16 x 600 column in Dialysis Buffer. Peak fractions were combined and concentrated to 5 μM for analysis by HDX-MS.

Neddylation reactions following purification of all necessary components resulted in only partial neddylation of CUL5-containing complex. We overcame this limitation by neddylating the CUL5-containing complex during its purification. Lysates for NAE1/UBA3 and NEDD8 were mixed with 10 mM Mg-ATP to form the NAE1/UBA3~NEDD8 adduct, which was then purified by NiNTA chromatography taking advantage of the His-tag on NEDD8 and dialyzed. The lysate containing the CUL5 complex, the lysate containing UBE2F (the E2 for CUL5 neddylation) and the NAE1/UBA3~NEDD8 were then mixed with 10 mM ATP at 4 °C. Full neddylation of CUL5 occurred within 30 min at 4 °C. The neddylated CUL5 complex was purified from NAE1/UBA3, UBE2F, and excess NEDD8 by size exclusion chromatography on Superdex S200 in Dialysis buffer.

ARIH2 and CUL5 were evaluated for binding through size exclusion chromatography. ARIH2 was mixed with an equimolar amount of either ELOB/C-CUL5(NEDD8)-RBX2 or ELOB/C-CUL5- RBX2 and then the resulting mixture was separated by size exclusion. While the sample with neddylated CUL5 eluted as a mostly homogenous peak, the non-neddylated sample eluted in two clearly separate peaks. SDS-PAGE of the SEC fractions indicated that ARIH2 coeluted preferentially with neddylated CUL5.

GB1 was cleaved from CUL5 and MBP was cleaved from ARIH2 by adding TEV to the proteins at a 1:10 molar ratio and incubating at 4 °C for 24 hours. TEV and the cleaved tags were

removed by size-exclusion over a Superdex S200 Increase 10/300 column in 20 mM Tris-HCl pH 8.0, 100 mM NaCl, 5% Glycerol, 1 mM DTT.

Sample compositions were identified and characterized according to the presence of the desired proteins as assessed by size exclusion chromatography, SDS-PAGE (10-15% Acrylamide gels), and nanospray LC MS/MS on a Lumos mass spectrometer after trypsin digestion.

ELOB/C-CUL5-RBX2, ELOB/C-CUL5(NEDD8)-RBX2, ARIH2, and ELOB/C-CUL5(NEDD8)-RBX2-ARIH2 protein samples were individually prepared for analysis by HDX-MS. ELOB/C-CUL5-RBX2, ELOB/C-CUL5(NEDD8)-RBX2, and ARIH2 were expressed and purified as described above. ELOB/C-CUL5(NEDD8)-RBX2-ARIH2 was formed by combining the ELOB/C-CUL5-RBX2 and ARIH2 following neddylation of CUL5. The combined complex was isolated by size-exclusion over a Superdex S200 Increase 10/300 column in 20 mM Tris-HCL pH 8.0, 100 mM NaCl, 5% Glycerol, 1 mM DTT.

Hydrogen Deuterium Exchange. HDX-MS experiments were conducted using a Waters nanoACQUITY ultra-high pressure liquid chromatography (UPLC) system equipped with H/DX technology and a LEAP H/D-X PAL liquid handling system as previously described(25). The H_2O Buffer was composed of 20 mM Tris-HCl, pH 8.0, 100 mM NaCl, 5% Glycerol, and 1 mM DTT, matching the Size-Exclusion Buffer used in the final stage of purification for each protein sample. This Buffer was lyophilized and resuspended in D_2O (D_2O Buffer). A 4 µL portion of a 5 µM protein sample was incubated for 5 min at 25 °C and then mixed with 56 µL of H_2O Buffer as a control or D_2O Buffer for deuteration times of 15 s, 30 s, 45 s, 60 s, or 120 s. Measurement of amide exchange during this time regime best captures allosteric transitions (26).The reaction was quenched with 60 µL of Quench Buffer (3 M guanidine, 0.1% formic acid, pH 2.66) at 0°C. A portion of the quenched sample (50 µL) was injected into a sample loop and subsequently digested on an in-line pepsin column (Immobilized Pepsin, Pierce Inc.) at 15°C. BEH C18 Vanguard pre-column, separated by analytical chromatography (Acquity UPLC BEH C18, 1.7 µM,

1.0 × 50 mm, Waters Corporation) using a 7-85% acetonitrile in 0.1% formic acid over 7.5 min, and electrosprayed into the Waters SYNAPT G2Si quadrupole time-of-flight mass spectrometer. The mass spectrometer was set to collect data in the Mobility, ESI+ mode; mass acquisition range of 200–2,000 (m/z); scan time 0.4 s. Continuous lock mass correction was accomplished with infusion of leu-enkephalin (m/z = 556.277) every 30 s (mass accuracy of 1 ppm for calibration standard). For peptide identification, the mass spectrometer was set to collect data in MSE, ESI+ mode instead.

Experimental Design and Statistical Rationale. The peptides were identified from triplicate MS^E analyses of 5 μM ELOB/C-CUL5(NEDD8)-RBX2 and ARIH2 samples using PLGS 2.5 (Waters Corporation). Peptide masses were identified using a minimum number of 250 ion counts for low energy peptides and 50 ion counts for their fragment ions. Peptides masses were identified using a minimum number of 250 ion counts for low energy peptides and 50 ion counts for their fragment ions; the peptides also had to be larger than 1500 Da.

The peptides identified in PLGS were then used to analyze the deuterium uptake in DynamX 3.0 (Waters Corporation) by first applying additional filters in DynamX 3.0 including a cut-off score of 6.5, minimum products per amino acid of 0.2, maximum MH+ error tolerance of 5 ppm, retention time standard deviation of 5%, and requiring that the peptide be present in at least 2 of the 3 peptide identification runs. Every mass envelope was manually checked. The deuterium uptake for each peptide was calculated by comparing the centroids of the mass envelopes of the deuterated samples vs. the undeuterated controls (27). For all HDX-MS data, at least 2 biological replicates were analyzed, each with 3 technical replicates. Data are represented as mean values +/- SEM of 3 technical replicates due to processing software limitations, however biological replicates were highly reproducible due to use of the LEAP robot for all experiments. The deuterium uptake was corrected for back-exchange using a global back exchange correction factor (typically 25%) determined from the average percent exchange measured in disordered termini of the sample proteins (28). ANOVA analyses and t tests with a p value cutoff of 0.05

implemented in the program, DECA (github.com/komiveslab/DECA), were used to determine the significance of differences between HDX data points (29). The peptides reported on the coverage maps are actually those from which deuterium uptake data were obtained. Deuterium uptake plots were plotted in DECA as number of deuterons incorporated vs. time (min). The Y-axis limit for each plot reflects the total possible number of amides within the peptide that can exchange. The uptake curves were fitted with an exponential curve for ease of viewing.

Ubiquitylation Reactions. Ubiquitylation reactions were carried out in a buffer containing 20mM Tris-HCl pH 7.5, 5 mM $MgCl_2$, 0.5 mM DTT, and 2 mM ATP with 0.5 μM UBE1, 5 μM UBE2D2 or UBE2R1 and/or ARIH2+UBE2L3, 100-200 uM Ub, and 5 μM ASB9-CRL as previously described (30). Reactions were incubated at 37 °C for 3 hours to ensure complete reaction (12), although substantial ubiquitin transfer was observed by 20 min. Reactions were subsequently quenched with reducing SDS-PAGE buffer, boiled at 90 °C for 10 minutes prior to SDS PAGE.

Thioester transfer of ubiquitin between UBE1 and UBE2D2 or UBE2R1 and/or ARIH2+UBE3L3, as well as the covalent ubiquitylation of CKB, was measured by monitoring the molecular weights of the proteins as previously described (31). Samples were separated by 10% polyacrylamide SDS-PAGE in replicate for parallel detection by Coomassie Blue staining and by anti-Ub Western Blotting using standard approaches. The blot was incubated overnight with rocking at 4 °C with mouse anti-Ub Antibody (Sigma 042691GS) diluted 1:4500 in blocking buffer, rabbit Anti-NEDD8 Antibody (CST 2754) diluted 1:4500 in Blocking Buffer, or rabbit Anti-Creatine kinase B type Antibody (Abcam ab38211) diluted 1:500 in Blocking Buffer. The blot was washed three times with TTBS (TBS with 0.05% Tween) and then incubated with secondary antibody Anti-Mouse IgG (H+L), HRP Conjugate (Promega W4021) or Anti-Rabbit IgG (H+L), HRP Conjugate (Promega W4011) for 1 hour with rocking at 23 °C. The blot was washed twice with TTBS and finally with TBS, developed by incubation with Bio-Rad Clarity Western ECL Substrate (1705061) for 5 min at 23 °C and imaged using a Bio-Rad Chemi-Doc. The Colorimetric Blot default protocol

was used to image the molecular weight ladder and the Chemi High Resolution Blot default protocol was used to detect chemiluminescence with exposures from 1-10 s.

ImageJ Gel Analysis. Coomassie stained gels and anti-CKB blots were imported into ImageJ (32). The background signal was subtracted from each lane, areas were calculated from each peak and data were plotted gel mobility vs. intensity.

NanoLC Mass Spectrometry for ubiquitin analysis. Ubiquitylation reaction samples were electrophoresed on 10% Tris-SDS poly-acrylamide gels in SDS gel running buffer for 5 min at 180 V. The gel lanes were excised from the bottom of the stacking gel to the dye front. For mass spectrometry of individual gel bands, samples were separated on 4–15% Mini-PROTEAN® TGX™ Precast Protein Gels (Bio-Rad 4561083) in SDS gel running buffer for 60 min at 180 V. After staining for 10 min in 0.25% w/v Coomassie Blue/40% MeOH/10% Acetic Acid and de-staining for 10 min in 20% MeOH/10% Acetic Acid, the gel bands were excised, cut into small pieces, and washed according to standard procedures(33). The proteins were acetylated, then the cysteines were reduced and alkylated with iodacetamide, and finally the proteins were digested with trypsin for 45 min at 4°C, then 37 °C overnight. The supernatant containing the tryptic peptides was collected and remaining peptides were extracted from the gel according to standard procedures (33). The samples were dried in a speed vac, and stored at -20 °C until analysis.

Trypsin-digested samples were analyzed by UPLC coupled with tandem mass spectroscopy (LC-MS/MS) using nano-spray ionization on an Orbitrap fusion Lumos hybrid mass spectrometer (Thermo) interfaced with nano-scale reversed-phase UPLC (Thermo Dionex UltiMate™ 3000 RSLC nano System) using a 25 cm, 75-micron ID glass capillary packed with 1.7-µm C18 (130) BEHTM beads (Waters corporation) and separated on a linear gradient (5–80%) of ACN at a flow rate of 375 nl/min for 1h in 0.1% formic acid. Mass spectrometer parameters are as follows; an MS1 survey scan using the orbitrap detector (mass range (m/z): 400-1500 (using quadrupole isolation), 120000 resolution setting, spray voltage of 2200 V, Ion transfer tube

temperature of 275 C, AGC target of 400000, and maximum injection time of 50 ms) was followed by data dependent scans (top speed for most intense ions, with charge state set to only include +2-5 ions, and 5 second exclusion time, while selecting ions with minimal intensities of 50000 at in which the collision event was carried out in the high energy collision cell (HCD Collision Energy of 30%), and the fragment masses where analyzed in the ion trap mass analyzer (With ion trap scan rate of turbo, first mass m/z was 100, AGC Target 5000 and maximum injection time of 35ms). Protein identification and label free quantification was carried out using Peaks Studio 8.5 (Bioinformatics solutions Inc.) The Human Uniprot Database (May 10, 2020) was searched with trypsin unspecific protease specificity allowing three missed cleavages. The fixed modifications were Carbamidomethylation (C), Acetylation (K, N-term) and the variable modifications were Ubiquitin (K) and PEAKS PTM open search. The precursor mass tolerance was 40 ppm and the fragment mass tolerance was 0.5 Da. The Score cutoff was -10 log P > 15. Digestion of a ubiquitinylated peptide by trypsin leaves a 'digly' modification with a mass of 114.04 Da on the ubiquitylated lysine (34). To quantify the amount of Ub at each lysine in CKB, the sum of the areas of all peptides with a digly at a particular lysine was divided by the sum of the areas for all peptides covering that lysine and these values were used for relative comparison between samples.

Homology Modeling. A model of ASB9-CRL with neddylated CUL5 was prepared by superimposing homologous domains of known structures to position each component in PyMOL. The CKB-ASB9-ELOB/C-CUL5NTD structure described in Lumpkin et al, 2020 (16). To orient the CUL5CTD relative to CUL5NTD, CUL2 from CUL2-RBX1-ELOB/C-VHL (5N4W) was first aligned to residues 306-387 on CUL5NTD in the starting model using PyMOL. CUL5CTD from CUL5CTD(NEDD8)-RBX1 (3DQV) was aligned to residues 383-424 on CUL2 from CUL2-RBX1-ELOB/C-VHL (5N4W). Following orientation of the two halves of CUL5, CUL2-RBX1-ELOB/C-VHL was removed from the model. Residues 208-238 of RNF4 in RNF4-UBE2D1-Ub (4AP4) were aligned to RBX1 to position UBE2D1-Ub, and RNF4 was removed. Prior to model refinement, sequences extracted from the PDBs were aligned to the full-length Human sequences

for each protein using the pairwise alignment tool EMBOSS Water from EMBL-EBI. The model by MODELLER (33), using the sequence alignments, to minimize loop energies, fill sequence gaps, correct solubility mutations, and to model RBX2 from RBX1. MODELLER 9.23 was run using the default automodel class. The model with the lowest MOLPDF score of the 10 models generated was selected as the final model.

ARIH2 was aligned to the sequence of ARIH1 extracted from the crystal structure of the ARIH1-UBE2L3-Ub complex (PDB 5UDH) using the pairwise alignment tool EMBOSS Water from EMBL-EBI. Zinc chelating residues C186, C189, C203, H205, C208, C211, C231, C236, C276, C281, C297, C299, C304, C307, H312, C317, C344, C347, C357, C362, C367, C372, C375, H382, and C389 in ARIH1 correspond to residues C139, C142, C156, H158, C161, C164, C183, C188, C228, C233, C249, C252, C257, C260, H265, C270, C297, C300, C310, C315, C318, C323, C326, H333, and C340 in ARIH2. The two protein sequences were aligned so that the Zinc-chelating residues were exactly aligned. Analysis of the ARIH2 sequence using NetSurfP 2.0 predicted residues 66-83, 88-97, 102-111, 113-120, 162-174, 194-200, 204-220, 257-260, 271-277, 281-293, 349-400, 404-434, 440-491 to be helical. Residues 66-84, 88-98, 102-110, 113-120, 148-150, 162-172, 194-200, 204-221, 270-281, 361-399, 404-433, and 438-491 were modeled as helical from alignment with ARIH1. ARIH2 residues 281-293 were predicted to be part of a longer helix extending from residue 271, however this segment is shorter in ARIH1, and was therefore modeled as a loop in ARIH2. A similar situation applied to ARIH2 residues 349-360. Substitution of ARIH2 for ARIH1 gave the structure of ARIH2-UBE2L3-Ub based on the structure of the complex (PDB 5UDH).

Docking the N-terminus of ARIH2 into ASB9-CRL. The flexible N-terminus of ARIH2 was docked onto ASB9-CRL using GalaxyWEB PepDock (35), CABS-dock (36), and HPEPDOCK (37). These docking programs were selected for their ability to model long peptides (>20 aa) in large proteins (>300 aa) and to discriminately score various models. HPEPDOCK performs blind peptide-protein docking of a given sequence to a submitted structure and returns models with

calculated docking energies. PepDock uses template structures of peptide-protein interactions to predict binding interfaces between the given peptide sequence and protein structure and scores the models based on protein and interaction similarities to the template. CABS-dock simulates and clusters trajectories of the given peptide sequence interacting with the submitted protein structure, returning the predominant clusters with RMSD scores, cluster density, and contact maps.

The peptide 'MSVDMNSQGSDSNEEDYDPNCEEEEEEEEDDPGDIEDYYVGVASDVEQ QGADAFDPE', corresponding to residues 1-57 of ARIH2, was docked onto CUL5(NEDD8)-RBX2, from the post-neddylation homology model, using HPEPDOCK. Ten models were generated, but the structures had little in common with each other and with insignificant contact with CUL5. The peptide 'DSNEEDYDPNCEEEEEEEEDDPGDIEDYYV', corresponding to residues 11-40 of ARIH2, was docked onto $CUL5_{1-780}$-RBX2 from the post-neddylation homology model, using PepDock (35). Docking with PepDock produced 10 models from four protein-peptide template structures. A particular region of $CUL5_{CTD}$ to which ARIH2 residues 11-40 preferentially docked was identified. However, the Estimated Accuracy score for all of the models was less than 0.4, indicating that less than 40% of the residue interactions in each model were likely to be correct. Furthermore, many of the docked structures seemed improbable because the ARIH2 sequence was threaded through CUL5. In addition, the ARIH2 sequences that were not threaded had contacts with CUL5 that did not match previous mutagenesis.

The peptide 'DSNEEDYDPNCEEEEEEEEDDPGDIEDY', corresponding to residues 11-38 of ARIH2 (truncated due to peptide length limitations), was docked onto $CUL5_{300-780}$ (truncated due to protein length limitations), from the post-neddylation homology model, using CABS-dock. Fifty simulation cycles were performed, and 10 models were generated. The model with the highest cluster density and no steric clashes with CUL5 was selected as the best model.

Building ARIH2 onto ASB9-CRL. The best CABS-dock model, consisting of residues 11-38 of ARIH2 bound to CUL5, was selected to begin building ARIH2 onto the full ASB9-CRL

homology model. Residues 34-60 of ARIH2 were modeled using PEP-FOLD3 (38). The model with the lowest sOPEP energy score was chosen. The docked peptide, the PEP-FOLD3 peptide, and the homology model for ARIH2 were used to model ARIH2 onto the ASB9-CRL homology model. MODELLER 9.23 was run using the default automodel class. The model with the lowest MOLPDF score of the 10 models generated was selected as the final model.

Results

Assembly of an active ASB9-CRL from purified proteins in vitro. Using a process of strategic co-expression and *E. coli* lysate mixing, we were able to assemble the following partial and complete ASB9-CRL protein complexes; CKB-ASB9-ELOB/C-CUL5(+/-NEDD8)-RBX2, CUL5(NEDD8)-RBX2, ARIH2-CUL5(NEDD8)-RBX2, as well as ARIH2 alone (Figure 1B, Supp. Figure 1). Neddylation did not require the CKB-ASB9 components and proceeded efficiently by mixing the *E.coli* lysate containing the CUL5 complex, the pre-formed NAE1/UBA3~NEDD8 adduct, and the NEDD8 E2, UBE2F with Mg ATP. Full CUL5 neddylation occurred within 30 min at 4 °C (Supp. Figure 2, see Methods for more details). To assess the thioester transfer of Ubiquitin to E2 enzymes (E2~Ub) we mixed UBE1 and an E2 enzyme with Ub (30) for 3 hr at 37 °C and measured band shifts by SDS-PAGE (31) and anti-Ub Western Blotting. The K724R mutant of CUL5 was used for non-neddylated CUL5 control experiments because we observed Ub could be attached to CUL5 K724 in the absence of NEDD8 and UBE2F by UBE2D2.

ARIH2 promotes CKB ubiquitylation. Consistent with a recent report, ARIH2 bound CUL5(NEDD8) with higher affinity compared to un-neddylated CUL5 (Supp. Figure 3) (22). Addition of ARIH2 and its ubiquitylated E2, UBE2L3~Ub, resulted in 50% of the CKB being ubiquitylated according to SDS PAGE (Figure 2A). If only UBE2D2 or UBE2R1 was added to CKB-ASB9-ELOB/C-CUL5(+NEDD8)-RBX2, the ratio of CKB to ASB9 remained 2:1 (Figure 2A, lanes 1-4) whereas addition of ARIH2 and UBE2L3~Ub resulted in migration of one equivalent of the CKB band to higher molecular weight, apparently due to ubiquitylation of one subunit of the dimeric CKB (Figures 2A and 2B (lanes 5-10). Notably, we never observed

migration/ubiquitylation of more than one equivalent of the dimeric CKB across three independent biological replicate experiments, strongly supporting the idea that only one subunit of the CKB dimer is ubiquitylated.

To probe the role of E2 enzymes that bind via RBX2, we added either UBE2D2 or UBE2R1 with UBE1 and Ub to the purified ligase (Figure 2C). In three separate biological replicates we observed that without ARIH2, the ratio of CKB:ASB9 was 1.9 ± 0.3 whereas with ARIH2 (alone or with UBE2D2 or with UBE2R1), the CKB:ASB9 ratio was 1.2 ± 0.4 indicating the migration of one equivalent of the dimeric CKB to higher molecular weight.

To measure ubiquitylation of specific lysines, we took advantage of the fact that trypsin leaves a diglycyl fragment on the lysine that bore the Ub that is readily detectable by MS/MS sequencing (34). The *in vitro* ubiquitylation samples were acetylated and analyzed by MS/MS. After trypsin digestion, approximately 200 peptides were observed from CKB that covered 93% of the CKB sequence and all but one (K319) of the 18 lysines. By comparing the total intensity of acetylated peptide vs. ubiquitylated peptide, we could obtain information about the likelihood that each lysine was ubiquitylated. Remarkably, very few of the 18 lysines were observed to be ubiquitylated (Supplementary Table 1). The most highly modified sites were K45 and K381, but K101 and K107 were also modified. MS/MS analysis also revealed which lysines of ubiquitin were linked. The ligase with ARIH2 either alone or with UBE2D2 or UBE2R1 produced a mixture of K48 and K63 Ub chain linkages on the same four lysines (Supplementary Table 2). MS/MS data collected on the high molecular weight species (cf. Figure 2C) showed only CKB and Ub in different ratios with the highest ratio of Ub to CKB present when ARIH2 and UBE2R1 were present suggesting that the combination of ARH2 and UBE2R1 generated the most polyubiquitylation.

Models of the structures of the neddylated ASB9-CRL with ARIH2 bound. Using a combination of cryoEM data and homology modeling, we previously obtained a model of the CKB-ASB9-ELOB/C-CUL5-RBX2 complex in which the CUL5 was not neddylated (16). Here, we used homology modeling to generate the structure of the $CUL5_{CTD}$(NEDD8)-RBX2 based on the

structure of $CUL5_{CTD}$(NEDD8)-RBX1 (PDB 3DQV), by aligning residues 208-238 of RNF4 in RNF4-UBE2D1-Ub (4AP4) to RBX1 to position UBE2D1-Ub. Finally, RBX1 was replaced with RBX2. The model has UBE2D1, which is very similar to UBE2D2 (89% identity, 97% similarity) and both E2s functioned in our ubiquitylation assays.

A homology model of ARIH2 was built based on the structure of ARIH1 (5UDH) by prioritizing the residues that coordinate the two zinc atoms in the RING and In-Between-RING domains (Supp. Figure 4). The interaction of ARIH2 with CUL5 was shown by mutagenesis to depend on residues R417, K418, K423, K424, K676, K679, K682, and R683 (21). Therefore, we used CABS-DOCK to dock the acidic N-terminal residues 11-38 of ARIH2 to this basic patch on CUL5 (36) (Figure 3A). ARIH2 contains additional residues (34-60) not present in ARIH1 which were modeled to complete the predicted structure of ARIH2, which was then assembled with CKB-ASB9-ELOB/C-CUL5(NEDD8)-RBX2. The final model of the ARIH2-bound to the ASB9 CRL showing the ubiquitylated CKB residues K45, K101, K107 and K381 is shown in Figure 3B. The four lysines that we found to be ubiquitylated appear to be the CKB surface lysines closest to the ARIH2. In line with our observation that only one subunit of CKB gets modified (see above), one subunit of CKB is much closer to ARIH2 than the other.

Both ARIH2 and RBX2 appear to be flexibly tethered to CUL5. Both ARIH2 and RBX2 have segments that are predicted to be unstructured that tether them to CUL5. HDX-MS measurements of deuterium uptake revealed that these apparent tethers, residues 46-58 of ARIH2 and residues 41-47 of RBX2 are highly exchanging even after only 30 s of exchange (Figure 4) consistent with a lack of structure. These tethers are likely to be important for optimal orientation for transfer of the Ub which would be attached to either ARIH2 or to one of the other E2s bound to RBX2.

Neddylation restructures CUL5 and RBX2. Neddylation of CUL5 is known to play an important role in the activation and regulation of CUL-RING ligases (39). Crystal structures of the C-terminal domain of CUL5 before and after neddylation show that the modification reorients the

C-terminal domain of CUL5 and increases the angle between CUL5 and RBX1 (3DPL, 3DQV). We performed HDX-MS experiments on CKB-ASB9-ELOB/C-CUL5-RBX2 and CKB-ASB9-ELOB/C-CUL5(NEDD8)-RBX2 to discover possible long-range conformational alterations that may occur upon neddylation. When CUL5 was neddylated, CUL5 residues 439-450, 489-496, 497-504, and 698-709 exchanged more, implying increased dynamics and/or solvent exposure of these regions (Figure 5, Supp. Figure 6). We note that CUL5 neddylation did not cause any observable decreases in exchange. Only 82% of the CUL5 sequence was covered in our HDX-MS data and residues 711 to 725 were not covered, so it is possible that NEDD8 contacts the surface of CUL5 near its attachment site. A completely unexpected decrease in exchange of RBX2 residues 52-58 was observed when neddylated CUL5-RBX2 was compared to unneddylated CUL5-RBX2. This RBX2 sequence is solvent exposed in the homology models both before and after neddylation. This region contains Arg 54, which by analogy with RBX1 is the linchpin residue (Arg 46 in RBX1) which is inserted between the NEDD8 and its E2 in the structure of the analogous proteins (PDB code 4P50, Supp. Figure 5).

ARIH2 binding to the ASB9-CRL causes decreased exchange in CUL5 and significantly increased exchange in ARIH2. Next, we compared free ARIH2 and free ELOB/C-CUL5(NEDD8)-RBX2, to the complex between them (ELOB/C-CUL5(NEDD8)-RBX2-ARIH2) by HDX-MS. The ARIH2 peptides containing the highly acidic residues that our docking (and the published mutagenesis experiments (21)) predict should interact with the positively charged patch on the C-terminus of CUL5 were not detected in the HDX-MS experiments. We did not identify any other surface of ARIH2 that showed decreased exchange upon binding to the CRL. On the other hand, comparison of deuterium uptake into the ELOB/C-CUL5(NEDD8)-RBX2 and ELOB/C-CUL5(NEDD8)-RBX2-ARIH2 complexes revealed CUL5 residues 333-344, 366-383, 415-429, 439-450, 465-471, 477-488, 528-544, and 639-648 decreased exchange in the presence of ARIH2. Interestingly, this effect was transient, disappearing by the 2 min timepoint (Figure 6, Supp Figure 7). We recall that neddylation caused increased exchange in CUL5 at regions 439-450

and 489-504, at or between the same areas that then decreased exchange upon ARIH2 binding. The protection of these regions of CUL5 upon ARIH2 binding is consistent with our docked model which places ARIH2 residues 11-38 in this cleft on CUL5 that is opened up by neddylation.

Finally, several regions of ELOB/C-CUL5(NEDD8)-RBX2-bound ARIH2 (residues 361-367, 369-381, 382-395, 404-413) showed marked increases in deuterium exchange compared to free ARIH2 (Figure 7, Supp Figure 8). These regions are near the catalytic cysteine and surround the domain of ARIH2 that has been previously reported to be autoinhibited prior to CUL5 binding (21). These results strongly indicate a long-range allosteric mechanism by which ARIH2 autoinhibition is released upon interaction with CUL5 which involves increased dynamics/exposure of these ARIH2 regions which surround the ARIH2 active site.

Discussion

Activity and specificity of the ASB CRL. We were able to reconstruct the full ASB9-CRL *in vitro* from recombinant proteins purified from *E. coli* and demonstrate efficient CKB ubiquitylation. The CUL5-RBX2 was readily neddylated in the absence of the substrate receptor (ASB9) and substrate (CKB) suggesting that substrate engagement is not required for CRL neddylation. ARIH2 was found to be critical for high efficiency ubiquitylation of the substrate, CKB. Indeed, ARIH2 is essential for ubiquitylation of a number of important substrates, such as APOBEC3 by the $CUL5^{Vif/CBF\beta}$ E3 ligase (22). Although others have suggested that ARIH2-UBE2L3 only installs the first Ub and then the polyubiquitin chain is elongated by the E2 bound to RBX2 (23), our results show that ARIH2-UBE2L3~Ub bound with high affinity to the neddylated CRL, and rapidly polyubiquitylated one equivalent of the CKB dimer at four specific lysines creating both K48 and K63 linked polyubiquitin chains on CKB. Addition of UBE2R1 or UBE2D2 supplemented ubiquitylation but these E2s could not efficiently ubiquitylate CKB in the absence of ARIH2.

Structural model of the ARIH2-bound ASB-CRL. Based on a previous structure of the ASB9-CRL (16) and previous mutagenesis experiments (21), ARIH2 was docked to form a

predicted structure of the full neddylated ASB9-CRL with ARIH2 bound. HDX-MS experiments identified several regions of CUL5 that increased in exchange upon neddylation, and then decreased in exchange upon ARIH2 binding strongly suggesting a mechanism for how neddylation promotes ARIH2 binding (22). The observation that the decreased exchange in the $CUL5_{CTD}$ was transient for all regions suggests that even though the affinity of ARIH2 for CUL5 is high enough to observe co-elution in size exclusion chromatography, the interacting residues continue to exchange with solvent over time. This may be a function of the highly charged nature of the interaction.

The structural models and HDX-MS results show that both ARIH2 and RBX2 are both attached to CUL5 by flexible tethers, which could allow them to be in multiple locations further accommodating simultaneous binding and/or Ub transfer once the first Ub is attached to CKB by ARIH2.

Functional dynamics and allostery in the ASB CRL. Comparison of several states of the ASB9-CRL revealed differences in H/D exchange indicative of long-range allosteric mechanisms that activate the ligase. First, it is known that RBX2 associates with UBE2F for neddylation (40) of CUL5 at K724. Once this is accomplished, RBX2 needs to release UBE2F and bind a ubiquitylating E2. We found that CUL5 neddylation triggered decreased exchange in RBX2 at Arg54. By analogy with RBX1, this is the “linchpin” residue which inserts between the NEDD8 and its E2 in the structure of the analogous proteins (PDB code 4P50) (40). These results suggest that CUL5 neddylation may induce long-range conformational alterations in RBX2 to discourage binding of the NEDD8 E2 to RBX2. These HDX results suggest a long-range allosteric mechanism by which the specificity of RBX2 for different E2 enzymes changes following neddylation (41). This long-range allostery would need to pass through the ostensibly flexible tether linking RBX2 to CUL5. This type of allostery has been seen before in at least one other multi-domain protein (28). We find that the model where CRL may hinge in order to allow Ub transfer across the >60 Å distance between Ub and the substrate is insufficient to explain the ubiquitylation of CKB by the

ASB9-CRL. Instead, for substrates that are far away from the RBX2-linked E2~Ub, the RBRL, ARIH2-UBE2L3~Ub, is required.

Second, we found that although neddylation did not alter the substrate-receptor side of the ligase, it increased the solvent exposure of the cleft where ARIH2 binds. This observation suggests that CUL5 is autoinhibited for high affinity ARIH2 binding until it is neddylated. NEDD8 attachment allosterically opens the CUL5 cleft into which ARIH2 binds, strengthening the ARIH2 binding affinity. ARIH2-UBE2L3 was necessary and sufficient for high efficiency poly-ubiquitylation of the substrate, CKB, which binds to the N-terminal end of ASB9 and would be too far from the RBX2-E2~Ub, at least initially.

Third, comparison of free ARIH2 and the ASB9-CRL-ARIH2 complex revealed that the interaction between ARIH2 and CUL5 markedly increased the dynamics of regions of the Ariadne domain surrounding the ARIH2 active site. It is interesting to speculate that somehow the UBE2L3~Ub can only be transferred to C310 in the Ariadne domain of ARIH2, once this region is opened when the ARIH2 engages with CUL5. Binding of the ARIH2 N-terminal acidic sequence to the CUL5 basic cleft apparently induces a long-range allosteric mechanism which releases the ARIH2 autoinhibition, presumably by increasing access to the catalytic cysteine. All of these allosteric changes allow ARIH2 to ubiquitylate substrates on the ASB9-CRL.

Conclusions. By comparing *in vitro* activity, structures, and HDX-MS dynamics of the ASB9-CRL, we were able to answer key mechanistic questions and propose a model of how neddylation of CUL5 E3 ligases are activated for ubiquitylation (Figure 8). 1) Neddylation of CUL5 allosterically signals to the CUL5-bound RBX2 that the ligase is already neddylated by discouraging its binding to another UBE2F, while allowing its binding of UBE2D2 or UBE2R1 to ubiquitylate substrates. 2) Neddylation of CUL5 allosterically opens the channel into which the N-terminal disordered acidic segment of ARIH2 binds. 3) ARIH2 binding to CUL5 allosterically opens the ARIH2 active site releasing its autoinhibition. ARIH2 efficiently ubiquitylates CKB at specific lysines that are the closest ones to the ARIH2 active site. 4) Polyubiquitylation proceeds after

initial ubiquitylation by ARIH2-UBE2L3~Ub. Addition of UBE2D2 or UBE2R1 to RBX2 are not required for polyubiquitylation *in vitro*, but either can apparently augment the ARIH2 polyubiquitylation. The flexible tethers which connect ARIH2 and RBX2 to CUL5 may allow the additional RBX2-E2~Ub's to reach the already ubiquitylated substrate lysines to extend the poly-ubiquitin chains.

Data Availability

In the Supplementary Material we have provided all of the State Data Excel files that can be used to generate all of the uptake plots for all of the proteins and complexes reported here. To generate uptake plots automatically from state data, it is best to use DECA (https://github.com/komiveslab/DECA). MS/MS data for ubiquitylation including annotated spectra, and all HDX-MS data are available at massive.ucsd.edu under dataset MSV000084812.

username: MSV000084812_reviewer

password: a

Acknowledgements

This work was supported by NSF grant MCB 1817774 and by NIH grant S10 OD016234, RL acknowledges support from NIH T32 GM008326.

References

1. Komander, D., and Rape, M. (2012) The ubiquitin code. *Annu Rev Biochem* 81, 203-229
2. Akutsu, M., Dikic, I., and Bremm, A. (2016) Ubiquitin chain diversity at a glance. *J Cell Sci* 129, 875-880
3. Ohtake, F., Saeki, Y., Ishido, S., Kanno, J., and Tanaka, K. (2016) The K48-K63 branched ubiquitin chain regulates NF-kB signaling. *Mol Cell* 64, 251–266
4. Swatek, K. N., and Komander, D. (2016) Ubiquitin modifications. *Cell Res* 26, 399–422
5. Yau, R., and Rape, M. (2016) The increasing complexity of the ubiquitin code. *Nat Cell Biol* 18, 579–586
6. Kamura, T., Maenaka, K., Kotoshiba, S., Matsumoto, M., Kohda, D., Conaway, R. C., Conaway, J. W., and Nakayama, K. I. (2004) VHL-box and SOCS-box domains determine binding specificity for Cul2-Rbx1 and Cul5-Rbx2 modules of ubiquitin ligases. *Genes Dev* 18, 3055-3065
7. Heuze, M. L., Guibal, F. C., Banks, C. A., Conaway, J. W., Conaway, R. C., Cayre, Y. E., Benecke, A., and Lutz, P. G. (2005) ASB2 is an Elongin BC-interacting protein that can assemble with Cullin 5 and Rbx1 to reconstitute an E3 ubiquitin ligase complex. *J Biol Chem* 280, 5468-5474
8. Andresen, C. A., Smedegaard, S., Sylvestersen, K. B., Svensson, C., Iglesias-Gato, D., Cazzamali, G., Nielsen, T. K., Nielsen, M. L., and Flores-Morales, A. (2014) Protein Interaction Screening for the Ankyrin Repeats and Suppressor of Cytokine Signaling (SOCS) Box (ASB) Family Identify Asb11 as a Novel Endoplasmic Reticulum Resident Ubiquitin Ligase. *Journal of Biological Chemistry* 289, 2043-2054
9. Li, J., Mahajan, A., and Tsai, M. D. (2006) Ankyrin repeat: a unique motif mediating protein-protein interactions. *Biochemistry* 45, 15168-15178
10. Mosavi, L. K., Minor, D. L., Jr., and Peng, Z. Y. (2002) Consensus-derived structural determinants of the ankyrin repeat motif. *Proc Natl Acad Sci U S A* 99, 16029-16034
11. Debrincat, M. A., Zhang, J. G., Willson, T. A., Silke, J., Connolly, L. M., Simpson, R. J., Alexander, W. S., Nicola, N. A., Kile, B. T., and Hilton, D. J. (2007) Ankyrin repeat and suppressors of cytokine signaling box protein asb-9 targets creatine kinase B for degradation. *J Biol Chem* 282, 4728-4737
12. Kwon, S., Kim, D., Rhee, J. W., Park, J. A., Kim, D. W., Kim, D. S., Lee, Y., and Kwon, H. J. (2010) ASB9 interacts with ubiquitous mitochondrial creatine kinase and inhibits mitochondrial function. *BMC Biol* 8, 23
13. Balasubramaniam, D., Schiffer, J., Parnell, J., Mir, S. P., Amaro, R. E., and Komives, E. A. (2015) How the ankyrin and SOCS box protein, ASB9, binds to creatine kinase. *Biochemistry* 54, 1673-1680
14. Muniz, J. R. C., Guo, K. D., Kershaw, N. J., Ayinampudi, V., von Delft, F., Babon, J. J., and Bullock, A. N. (2013) Molecular Architecture of the Ankyrin SOCS Box Family of CuI5-Dependent E3 Ubiquitin Ligases. *Journal of Molecular Biology* 425, 3166-3177
15. Schiffer, J. M., Malmstrom, R. D., Parnell, J., Ramirez-Sarmiento, C., Reyes, J., Amaro, R. E., and Komives, E. A. (2016) Model of the Ankyrin and SOCS Box Protein, ASB9, E3 Ligase Reveals a Mechanism for Dynamic Ubiquitin Transfer. *Structure* 24, 1248-1256
16. Lumpkin, R. J., Baker, R. W., Leschziner, A. E., and Komives, E. A. (2020) Structure and dynamics of the ASB9 CUL-RING E3 Ligase. *Nat Commun.* 11, 2866

17. Baek, K., Krist, D. T., Prabu, J. R., Hill, S., Klügel, M., Neumaier, L. M., von Gronau, S., Kleiger, G., and Schulman, B. A. (2020) NEDD8 nucleates a multivalent cullin-RING-UBE2D ubiquitin ligation assembly. *Nature* 578, 461-466
18. Dove, K. K., and Klevit, R. E. (2017) RING-Between-RING E3 Ligases: Emerging Themes amid the Variations. *J Mol Biol* 429, 3363-3375
19. Duda, D. M., Olszewski, J. L., Schuermann, J. P., Kurinov, I., Miller, D. J., Nourse, A., Alpi, A. F., and Schulman, B. A. (2013) Structure of HHARI, a RING-IBR-RING ubiquitin ligase: autoinhibition of an Ariadne-family E3 and insights into ligation mechanism. *Structure* 21, 1030-1041
20. Scott, D. C., Rhee, D. Y., Duda, D. M., Kelsall, I. R., Olszewski, J. L., Paulo, J. A., de Jong, A., Ovaa, H., Alpi, A. F., Harper, J. W., and Schulman, B. A. (2016) Two Distinct Types of E3 Ligases Work in Unison to Regulate Substrate Ubiquitylation. *Cell* 166, 1198-1214.e1124
21. Kelsall, I. R., Duda, D. M., Olszewski, J. L., Hofmann, K., Knebel, A., Langevin, F., Wood, N., Wightman, M., Schulman, B. A., and Alpi, A. F. (2013) TRIAD1 and HHARI bind to and are activated by distinct neddylated Cullin-RING ligase complexes. *EMBO J* 32, 2848-2860
22. Huttenhain, R., Xu, J., Burton, L. A., Gordon, D. E., Hultquist, J. F., Johnson, J. R., Satkamp, L., Hiatt, J., Rhee, D. Y., Baek, K., Crosby, D. C., Frankel, A. D., Marson, A., Harper, J. W., Alpi, A. F., Schulman, B. A., Gross, J. D., and Krogan, N. J. (2019) ARIH2 Is a Vif-Dependent Regulator of CUL5-Mediated APOBEC3G Degradation in HIV Infection. *Cell Host Microbe* 26, 86-99 e87
23. Scott, D. C., Rhee, D. Y., Duda, D. M., Kelsall, I. R., Olszewski, J. L., Paulo, J. A., de Jong, A., Ovaa, H., Alpi, A. F., Harper, J. W., and Schulman, B. A. (2016) Two Distinct Types of E3 Ligases Work in Unison to Regulate Substrate Ubiquitylation. *Cell* 166, 1198-1214 e1124
24. Huttlin, E. L., Bruckner, R. J., Paulo, J. A., Cannon, J. R., Ting, L., Baltier, K., Colby, G., Gebreab, F., Gygi, M. P., Parzen, H., Szpyt, J., Tam, S., Zarraga, G., Pontano-Vaites, L., Swarup, S., White, A. E., Schweppe, D. K., Rad, R., Erickson, B. K., Obar, R. A., Guruharsha, K. G., Li, K., Artavanis-Tsakonas, S., Gygi, S. P., and Harper, J. W. (2017) Architecture of the human interactome defines protein communities and disease networks. *Nature* 545, 505-509
25. Narang, D., Chen, W., Ricci, C. G., and Komives, E. A. (2018) RelA-Containing NFkappaB Dimers Have Strikingly Different DNA-Binding Cavities in the Absence of DNA. *J Mol Biol* 430, 1510-1520
26. Markwick, P. R. L., Peacock, R. B., and Komives, E. A. (2019) Accurate Prediction of Amide Exchange in the Fast Limit Reveals Thrombin Allostery. *Biophys J* 116, 49-56
27. Wales, T. E., Fadgen, K. E., Gerhardt, G. C., and Engen, J. R. (2008) High-speed and high-resolution UPLC separation at zero degrees Celsius. *Anal Chem* 80, 6815-6820
28. Ramsey, K. M., Dembinski, H. E., Chen, W., Ricci, C. G., and Komives, E. A. (2017) DNA and IkappaBalpha Both Induce Long-Range Conformational Changes in NFkappaB. *J Mol Biol* 429, 999-1008
29. Lumpkin, R. J., and Komives, E. A. (2019) DECA, a comprehensive, automatic post-processing program for HDX-MS data. *Mol Cell Proteomics*
30. Choo, Y. S., and Zhang, Z. (2009) Detection of protein ubiquitination. *J Vis Exp*
31. Scheffner, M., Nuber, U., and Huibregtse, J. M. (1995) Protein ubiquitination involving an E1-E2-E3 enzyme ubiquitin thioester cascade. *Nature* 373, 81-83

32. Schneider, C. A., Rasband, W. S., and Eliceiri, K. W. (2012) NIH Image to ImageJ: 25 years of image analysis. *Nat Methods* 9, 671-675.
33. Villar-Garea, A., Israel, L., and Imhof, A. (2008) Analysis of histone modifications by mass spectrometry. *Curr Protoc Protein Sci* Chapter 14, Unit 14 10
34. Peng, J., Schwartz, D., Elias, J. E., Thoreen, C. C., Cheng, D., Marsischky, G., Roelofs , J., Finley, D., and Gygi, S. P. (2003) A proteomics approach to understanding protein ubiquitination. *Nat Biotechnol.* 21, 921-926
35. Lee, H., Heo, L., Lee, M. S., and Seok, C. (2015) GalaxyPepDock: a protein-peptide docking tool based on interaction similarity and energy optimization. *Nucleic Acids Res* 43, W431-435
36. Kurcinski, M., Badaczewska-Dawid, A., Kolinski, M., Kolinski, A., and Kmiecik, S. (2019) Flexible docking of peptides to proteins using CABS-dock. *Protein Sci*
37. Zhou, P., Jin, B., Li, H., and Huang, S. Y. (2018) HPEPDOCK: a web server for blind peptide-protein docking based on a hierarchical algorithm. *Nucleic Acids Res* 46, W443-W450
38. Lamiable, A., Thévenet, P., Rey, J., Vavrusa, M., Derreumaux, P., and Tufféry, P. (2016) PEP-FOLD3: faster de novo structure prediction for linear peptides in solution and in complex. *Nucleic Acids Res* 8, W449-454.
39. Lydeard, J. R., Schulman, B. A., and Harper, J. W. (2013) Building and remodelling Cullin-RING E3 ubiquitin ligases. *EMBO Rep* 14, 1050-1061
40. Scott, D. C., Sviderskiy, V. O., Monda, J. K., Lydeard, J. R., Cho, S. E., Harper, J. W., and Schulman, B. A. (2014) Structure of a RING E3 trapped in action reveals ligation mechanism for the ubiquitin-like protein NEDD8. *Cell* 157, 1671-1684
41. Duda, D. M., Borg, L. A., Scott, D. C., Hunt, H. W., Hammel, M., and Schulman, B. A. (2008) Structural insights into NEDD8 activation of cullin-RING ligases: conformational control of conjugation. *Cell* 134, 995-1006.
42. Lumpkin, R., Baker, R., Leschziner, A., and Komives, E. (2020) Structure and dynamics of the ASB9 CUL-RING E3 Ligase. *Nat Commun* 11, 2866

Figure Legends

Figure 1. *Schematics of the ubiquitylation cascade as mediated by the ASB9 CUL5 E3 ligase.* A) Ubiquitin is activated through a three-step enzymatic cascade. The Ubiquitin-activating enzyme (E1) binds ATP and catalyzes adenylation of Ubiquitin. The active-site cysteine on E1 attacks the Ub-AMP complex to form a thioester bond. Through a trans-thioesterification reaction Ubiquitin is transferred to the active-site cysteine on a Ubiquitin-conjugating enzyme (E2). Ubiquitin Ligases (E3) facilitate the highly specific covalent attachment of activated Ubiquitin (Ub) to bound substrate proteins through an isopeptide bond on an exposed lysine residue. B) Schematic showing the states of the ASB9-CRL explored in this work: un-activated, activated by NEDD8, and activated by NEDD8 with ARIH2 present. The protein abbreviations and colors are consistent throughout the manuscript: creatine kinase brain-type (CKB, two-tone teal); ankyrin and SOCS-box protein 9 (ASB9, yellow); Elongins B and C (ELOB/C, purple); cullin 5 (CUL5, salmon), ring box protein 2 (RBX2, olive); the ubiquitin conjugating enzyme bound to RBX2 (UBE2D1/2, magenta); ubiquitin (Ub, tan); Ariadne RBR E3 Ubiquitin Protein Ligase 2 Ring between Ring ligase (ARIH2 RBRL, orange); the ARIH2 RBRL ubiquitin conjugating enzyme (UBE2L3, grey). The Ub is transferred from UBE2L3 to ARIH2 prior to transfer to the substrate.

Figure 2. *In vitro ubiquitylation assays showing AriH2 induced ubiquitylation*. A) Coomassie blue-stained gel of various ubiquitylation reactions. All reactions contained MgATP, UBE1, and Ub. Lanes 1, 3, 5, 7, 9 contain CKB-ASB9-ELOB/C-CUL5-RBX2. Lanes 2, 4, 6, 8, 10 contain CKB-ASB9-ELOB/C-CUL5(NEDD8)-RBX2. Lane-specific additional components are: UBE2D2 (lane 1, 2), UBE2R1 (lanes 3, 4), ARIH2-UBE2L3 (lanes 5, 6), ARIH2-UBE2L3-UBE2D2 (lanes 7, 8), and ARIH2-UBE2L3-UBE2R1 (lanes 9, 10). B) Anti-CKB blot for the reactions as in panel A showing the increase in CKB migrating at high molecular weight. C) Image J analysis of the Anti-

CKB blot in B. The high molecular weight CKB ratioed against CKB reveals the most efficient combination of components for polyubiquitylation of CKB is ARIH2 with UBE2R1. Subsets of this experiment (biological replicates) were repeated three times.

Figure 3. *Model of the ASB9-CRL showing sites of ubiquitylation on CKB*. A) Molecular docking was used to place ARIH2 residues 11-38 into the basic cleft in CUL5. Acidic residues on ARIH2 are shown in red and CUL5 basic residues previously shown to be critical for the interaction (21) are shown in blue. B) A structural model of CKB-ASB9-ELOB/C-CUL5(NEDD8)-RBX2-E2D1/2~Ub-ARIH2-UBE2F~Ub built from the published structure of ASB9-ELOB/C-CUL5-RBX2-UBE2D1/2 (42) by addition of ARIH2-UBE2F~Ub based on the docked structure from A). Homologous structural information is not available until residue 57 of ARIH2, so the absolute position of ARIH2 relative to the ASB9-CRL is speculative. The four CKB lysines (K45, K101, K107, and K381) on one subunit of the monomeric CKB that were observed to be ubiquitylated (red side chains) are the closest lysines to ARIH2. The protein colors are consistent throughout the manuscript: CKB, aquamarine, dark cyan; ASB9, yellow; ELOB/C, orchid, purple; CUL5, rosy brown, RBX2, olive; NEDD8, chartreuse; UBE2D1/2, magenta; Ub on UBE2D1/2, khaki; ARIH2, orange, UBE2L3, grey; Ub on UBE2F, blue.

Figure 4. *HDX-MS reveals flexible tethers on ARIH2 and RBX2.* HDX-MS shows residues 46-58 of ARIH2 are highly exchanging when ARIH2 is alone (green) or bound to the ASB9-CRL (magenta). This segment of ARIH2 (orange) is colored in red in the structural model of the ASB9-CRL (expanded view). Similarly, RBX2 residues 41-47 are highly exchanging in the ASB9-ELOB/C-CUL5-RBX2 complex (brown) as well as in the Neddylated complex (black). This segment of RBX2 (olive) is also colored red in the structural model of the ASB9-CRL (expanded view).

Figure 5. *HDX-MS reveals long-range allostery upon neddylation of CUL5*. Comparison of the HDX-MS deuterium uptake into CKB-ASB9-ELOB/C-CUL5-RBX2 complex (brown symbols in plots) with the CKB-ASB9-ELOB/C-CUL5(NEDD8)-RBX2 complex (black symbols in plots) revealed that neddylation of CUL5 causes increased exchange in CUL5 residues (red) and decreased exchange in RBX2 residues (blue).

Figure 6. *HDX-MS reveals transient protection of CUL5 by the N-terminus of ARIH2.* Comparison of the HDX-MS deuterium uptake into ELOB/C-CUL5(NEDD8)-RBX2 complex (magenta symbols in plots) with the ELOB/C-CUL5(NEDD8)-RBX2-ARIH2 complex (black symbols in plots) revealed that the CUL5 regions that form the basic cleft and the surrounding residues are transiently protected upon ARIH2 binding (blue regions in structure).

Figure 7*: HDX-MS of AriH2 reveals the mechanism for relief of autoinhibition.* Comparison of the HDX-MS deuterium uptake into ARIH2 alone (red symbols in the plots) vs. in complex with the ASB9-CRL (black symbols in the plots) show marked increase in exchange (red regions in the structure) of the helical regions surrounding the ARIH2 active site upon binding to ASB9-CRL.

Figure 8. *Schematic diagram of the CRL E3 ligase mechanism based on the results of this study.* Our data support a mechanism by which RBX2 initially engages UBE2F to neddylate CUL5. Neddylation alters the RBX2 to decrease exchange at its binding site for UBE2F. Neddylation also alters the conformation of CUL5 opening a cleft of basic residues to which the acidic C-terminus of ARIH2 can bind with high affinity. ARIH2 is autoinhibited, but upon binding to CUL5, its active site increases exchange via a long-range allosteric mechanism (indicated by exposure of the -SH group). The increased exchange likely indicates opening of the ARIH2 active site and relief of autoinhibition. After initial Ub transfer by ARIH2 to specific lysines on

CKB that are close to the ARIH2 active site, polyubiquitylation on those same lysines can occur by a number of different routes including continued ubiquitylation by ARIH2, or contributions from UBE2D2 or UBE2R1 bound to RBX2.

Figure 1 Lumpkin et al

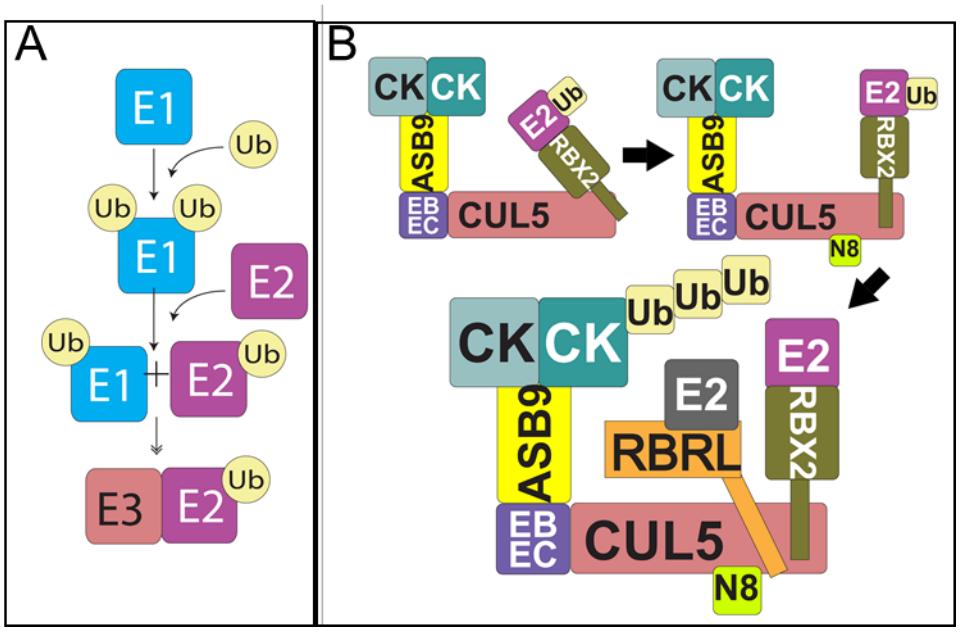

Figure 2 Lumpkin et al

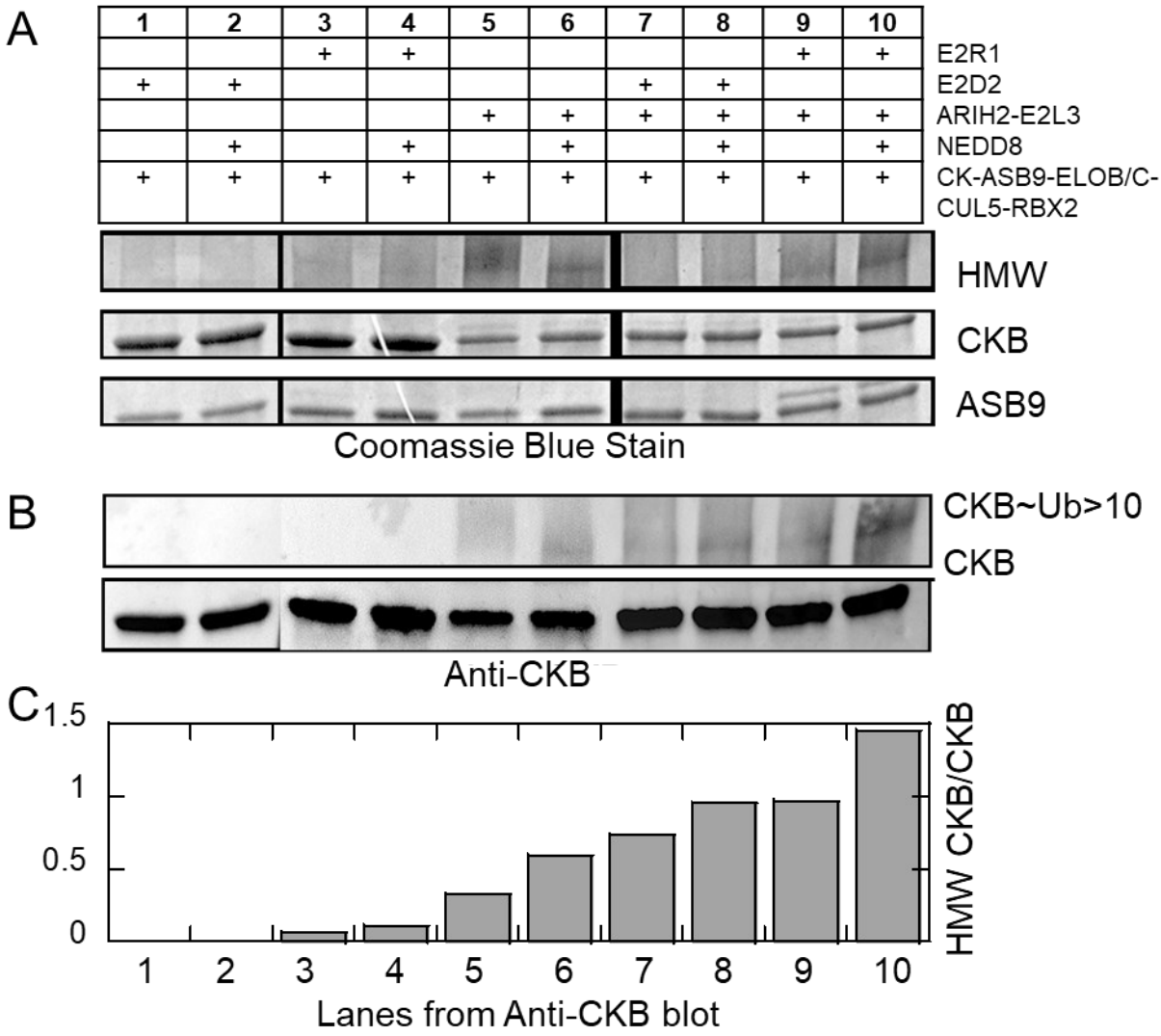

Figure 3 Lumpkin et al.

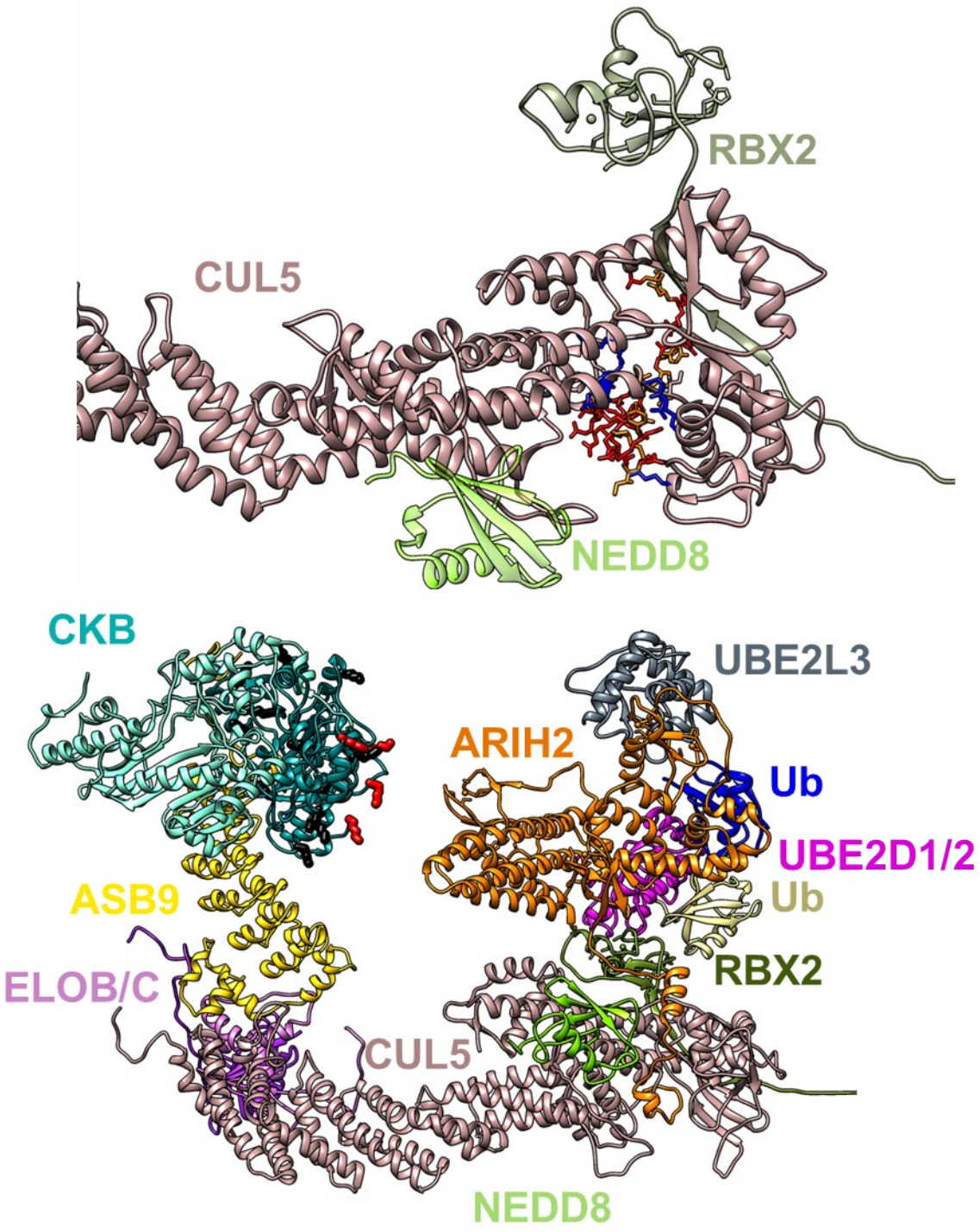

Figure 4. Lumpkin et al.

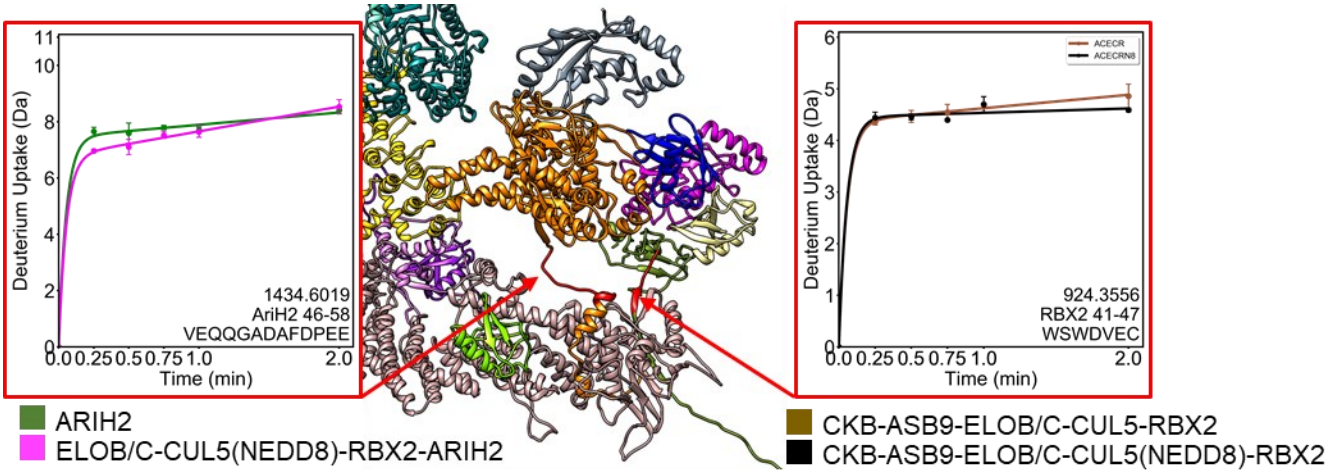

Figure 5 Lumpkin et al.

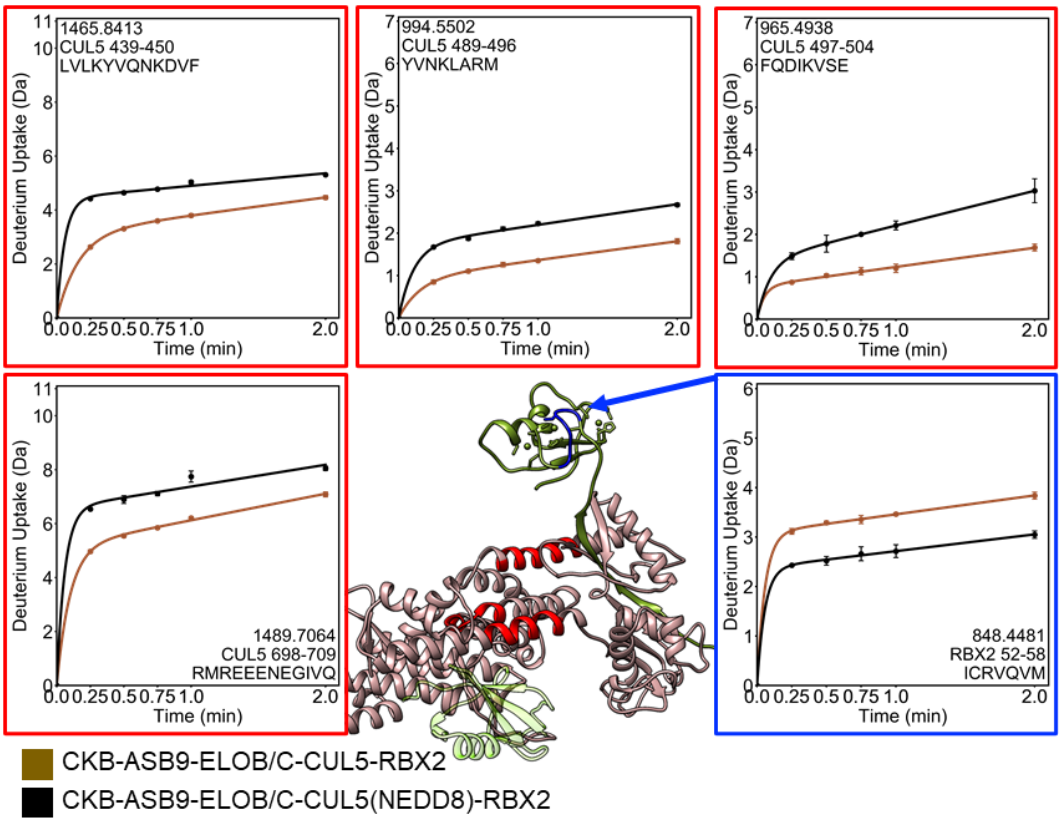

Figure 6 Lumpkin et al.

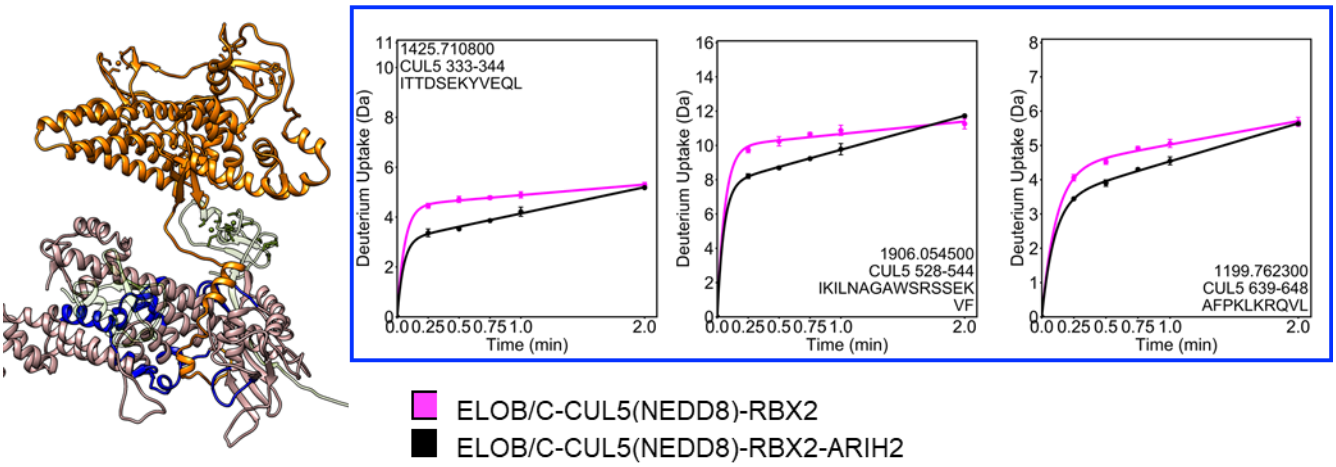

Figure 7 Lumpkin et al.

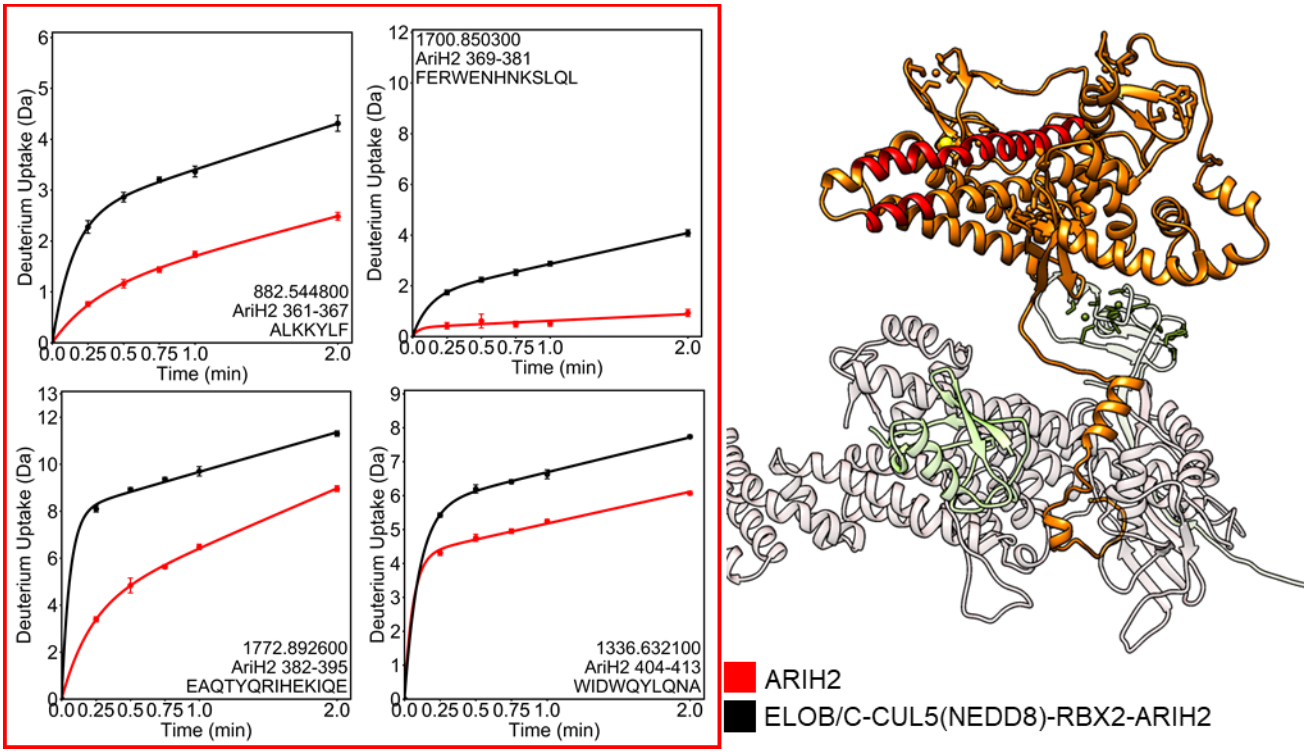

Figure 8 Lumpkin et al.